

# Lab on a Chip

Accepted Manuscript



This is an *Accepted Manuscript*, which has been through the Royal Society of Chemistry peer review process and has been accepted for publication.

*Accepted Manuscripts* are published online shortly after acceptance, before technical editing, formatting and proof reading. Using this free service, authors can make their results available to the community, in citable form, before we publish the edited article. We will replace this *Accepted Manuscript* with the edited and formatted *Advance Article* as soon as it is available.

You can find more information about *Accepted Manuscripts* in the [Information for Authors](#).

Please note that technical editing may introduce minor changes to the text and/or graphics, which may alter content. The journal's standard [Terms & Conditions](#) and the [Ethical guidelines](#) still apply. In no event shall the Royal Society of Chemistry be held responsible for any errors or omissions in this *Accepted Manuscript* or any consequences arising from the use of any information it contains.



Journal Name

ARTICLE

## Virtual Membrane for Filtration of Particles using Surface Acoustic Waves (SAW)

Armaghan Fakhfouri<sup>a</sup>, Citsabehsan Devendran<sup>a</sup>, David J. Collins<sup>b</sup>, Ye Ai<sup>b</sup>, Adrian Neild<sup>a</sup>

Received 00th January 20xx,  
Accepted 00th January 20xx

DOI: 10.1039/x0xx00000x

www.rsc.org/

Surface acoustic wave (SAW) based particle manipulation is contactless, versatile, non-invasive and biocompatible making it useful for biological studies and diagnostic technologies. In this work, we present a sensitive particle sorting system, termed a virtual membrane, in which a periodic acoustic field with a wavelength on the order of the particle dimensions permits size-selective filtration. Polystyrene particles that are larger than approximately 0.3 times the acoustic half-wavelength experience a force repelling them from the acoustic field. If the particle size is such that at a given acoustic power and flow velocity, this repulsive force is dominant over the drag force, these particles will be prohibited from progressing further downstream (i.e. filtered), while smaller particles are able to pass through the force field along the pressure nodes (akin to a filter's pores). Using this mechanism, we demonstrate high size selectivity using a standing SAW generated by opposing sets of focused interdigital transducers (FIDTs). The use of FIDTs permits the generation of a highly localized standing wave field, here used for filtration in  $\mu\text{L}/\text{min}$  order flow rates at 10's of mW of applied power. Specifically, we demonstrate the filtration of 8  $\mu\text{m}$  particles from 5  $\mu\text{m}$  and 10.36  $\mu\text{m}$  from 7.0  $\mu\text{m}$  and 5.0  $\mu\text{m}$  particles, using high frequency SAW at 258 MHz, 192.5 MHz, 129.5 MHz, respectively.

### Introduction

Separation and filtration of micron sized particles and cells is an essential step for various chemical and medical processes. In point-of-care diagnostic devices, for example, automated filtration of a specific type of cell from a biological samples is essential for further analysis, where microfluidic systems can perform this task with minimal reagent, time and cost. On-chip manipulation of suspended particles is accomplished using the advantageous characteristics of microscale flow, particularly the fluid viscous drag force. This is usually accompanied by application of an external force including those arising from optical<sup>1,2</sup> dielectrophoretic (DEP)<sup>3-5</sup> and acoustophoretic fields.<sup>6-8</sup> The interplay between these external forces and the drag forces induced by the flow field can be used to achieve particle separation. To date, the vast majority of these sorting strategies operate such that the particles are dragged through the force field by the flowing fluid, but follow distinct trajectories based on their different responses to an externally applied field, as such the streamline along which particles exit the force field is size dependant.<sup>9-16</sup> In addition, external fields have also be used

to non-selectively manipulate and trap suspended particles against a flow, this has demonstrated using mechanical,<sup>17, 18</sup> hydrodynamic,<sup>19</sup> optical,<sup>20, 21</sup> magnetic actuations<sup>22, 23</sup> and acoustic<sup>24-26</sup> techniques. Acoustic forces are particularly suitable for microfluidic actuation owing to their high biocompatibility<sup>27-30</sup> and straightforward microfluidic integration.

Here, we combine these features (sorting within a flow and trapping against a flow), by selectively filtering particles with a specific size profile from a mixed population. The trapped particles are held in a pre-determined position, offering potential for localised optical analysis, while the untrapped particles are allowed to flow through and out of the chip permitting the selective dispensing of one particle type out from mixed population.

Acoustofluidics, namely, the application of acoustic effects in microfluidic systems, utilises acoustic radiation forces (ARF) as a method for manipulating microparticles (suspended objects including cells). Particles immersed in a fluid with a different density and/or sound speed to the surrounding medium are subjected to ARF when they are exposed to an oscillating pressure and fluid displacement field. This effect arises from second order terms in the Navier-Stokes equation, which are non-zero when integrated over the particle's surface and time-averaged over an acoustic cycle.<sup>31, 32</sup> The time scale of ARF-induced migration is, therefore, much larger than the time period of an acoustic oscillation, though the maximum particle migration distance in a standing wave field scales with the wavelength of the pressure field. Typical methods exploiting ARF for size-based particle filtration utilize actuation based on bulk acoustic waves (BAW) or surface acoustic waves (SAW). The

<sup>a</sup> Laboratory for Micro Systems, Department of Mechanical and Aerospace Engineering, Monash University, Clayton, Victoria 3800, Australia. E-mail: Adrian.neild@monash.edu

<sup>b</sup> Engineering Product Design pillar, Singapore University of Technology and Design, Singapore.

† Footnotes relating to the title and/or authors should appear here.

Electronic Supplementary Information (ESI) available: [details of any supplementary information available should be included here]. See DOI: 10.1039/x0xx00000x

former is produced through exciting a resonance within the fluid volume.<sup>33-39</sup> ARF can be used for sorting by exploiting the difference in time (i.e. migration rate) required to move particles of various sizes to the pressure node in the standing wave field,<sup>40-42</sup> or the different behaviour of particles with differing material parameters,<sup>12</sup> where particles experience a difference in ARF magnitude based on their dimensions and physical properties. While the location and orientation of a BAW-generated wave is typically determined by the channel geometries and their acoustic properties (iso-impedance channel materials can be used to partially decouple the acoustic and channel interfaces<sup>34</sup>), a SAW is substrate-bound prior to coupling into contacting materials, and can thus be readily oriented and highly localized.<sup>43, 44</sup> A SAW is generated on a piezoelectric substrate by an alternating electrical current applied across a series of interdigital transducers (IDTs), whose micron-scale feature sizes result in 4-400  $\mu\text{m}$  wavelengths that are directly comparable to typical microfluidic channel dimensions. Accordingly, SAW has been widely used in microfluidics for activities including droplet production,<sup>32</sup> merging<sup>45</sup> and steering,<sup>46, 47</sup> atomization,<sup>48-50</sup> highly controllable particle manipulation<sup>43, 51, 52</sup> and mixing.<sup>53, 54</sup> Key features of SAW actuation have been exploited in sorting applications to cause particles to follow size dependant trajectories through the force field. SAW is similarly suited for size-selective sorting applications because of its ability to create highly localized fields,<sup>55, 56</sup> that are independent of the channel orientation<sup>6</sup> and the ability to utilise standing wave<sup>57</sup> or travelling wave<sup>58</sup> mechanisms, or a combination of both.<sup>59</sup> In addition, SAW actuation allows operation across a wide range of wavelengths ( $\sim 5\text{-}300\ \mu\text{m}$ ), the lower end of which means that wavelengths on the order of the cell dimensions can be excited.

Here we exploit the ability to generate small wavelengths on the order of the particle dimensions to selectively filter (and trap) one particle size from a mixed flowing particle suspension.

We utilize a standing pressure field established via actuation of counter propagating focused SAWs oriented at an angle of  $60^\circ$  to the flow direction. It is known that particles considerably smaller than the acoustic wavelength will migrate along pressure nodes to locations of maximum field strength.<sup>36</sup> We show that if a particle has a diameter greater than  $0.15\ \lambda_{\text{SAW}}$  the force along the nodal line switches sign and acts to repel the particle from the sound field. By balancing the acoustic power and flow rate we show experimentally that particles with a diameter similar to or greater than half the wavelength (i.e.  $\lambda_{\text{SAW}}/2$ ) are trapped statically, while smaller particles pass through the sound field along pressure nodes. The alignment of smaller particles as they pass through the field are as if along virtual pores projecting perpendicularly to the acoustic propagation axis. Coupled with the size based trapping effect, we accordingly term this acoustic field and its acoustofluidic interactions a virtual membrane.

Using this SAW-based virtual membrane we demonstrate continuous separation of  $5\ \mu\text{m}$  and  $3\ \mu\text{m}$ ,  $8\ \mu\text{m}$  and  $5\ \mu\text{m}$ ,  $10.36\ \mu\text{m}$  and  $7.0\ \mu\text{m}/5.0\ \mu\text{m}$ ,  $15\ \mu\text{m}$  and  $10\ \mu\text{m}/8\ \mu\text{m}$  diameter particles with actuation at 385.5 MHz, 258 MHz, 192.5 MHz, and

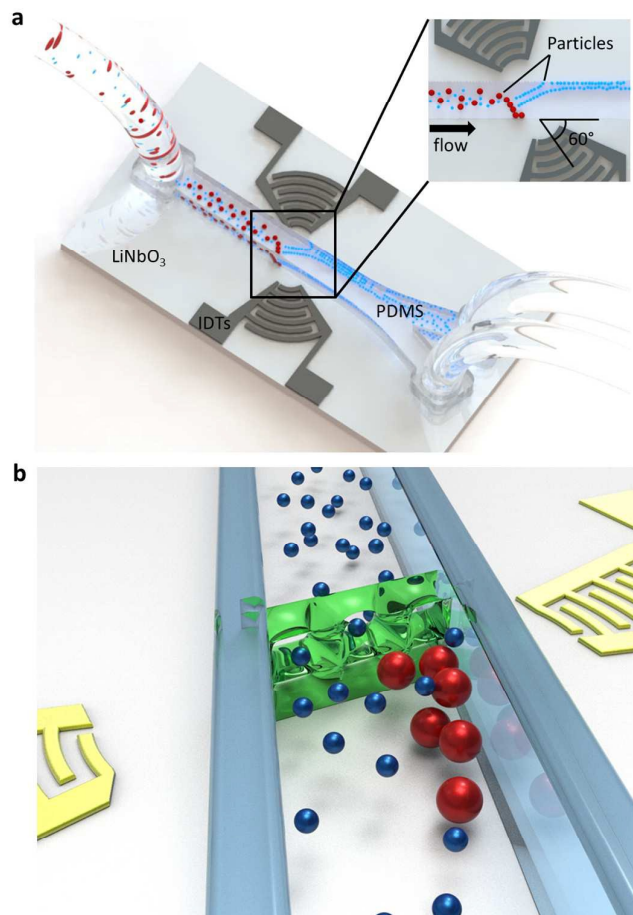


Fig. 1: (a) 3D rendered image of the virtual membrane for particle filtration system structure and the operation of the device: two diagonally opposed pairs of radially focussed interdigital transducers (FIDTs), arrayed on a Lithium Niobate ( $\text{LiNbO}_3$ ) substrate, oriented at a  $60^\circ$  angle relative to the flow direction confined within a straight PDMS microfluidic channel. An aqueous solution containing various-sized suspended particles enters an acoustic field created by focused IDTs where particles are influenced by the 2<sup>nd</sup> order time averaged absolute pressure field. Larger particles are trapped at beginning of the field, whereas smaller particles pass through pressure minima lines towards the upper boundary of the microfluidic chamber. (b) Zoomed-in image of the acoustic filtration region, whereby the virtual membrane (depicted in green) acts to filter the larger particles (red) while allowing the smaller particles (blue) to pass through the virtual pores.

129.5 MHz, respectively. In each case the frequency corresponds to a device pitch ( $\lambda_{\text{SAW}}/2$ ) of the larger particle diameter.

## Methodology

### Experimental Method

The device consists of a microfluidic channel, cast in polydimethylsiloxane (PDMS, 1:10 ratio of curing agent/polymer), and aligned on top of a SAW device. The SAW device is comprised of two diagonally opposed pairs of radially focussed interdigital transducers (FIDTs) on a Lithium Niobate ( $\text{LiNbO}_3$ ) piezoelectric substrate (Fig. 1). In the experiments

conducted, several devices with IDTs of varying wavelength were used in order to conclusively demonstrate the effect of acoustic wavelength on particle filtration. Three different IDT designs were used: 40 finger-pairs at  $20\mu\text{m}$  wavelength ( $\lambda_{\text{SAW}}$ ), 38 finger-pairs at  $15\mu\text{m}$  wavelength and 36 finger-pairs at  $10\mu\text{m}$  wavelength, all spanning  $26^\circ$  with a geometric focal point  $160\mu\text{m}$  from the last finger-pair. The  $7/200\text{ nm}$  chrome/aluminium IDTs were deposited on a  $0.5\text{ mm}$  thick, double side polished  $128^\circ$  y-cut x-propagating  $\text{LiNbO}_3$  substrate. A  $300\text{ nm}$   $\text{SiO}_2$  layer was further applied to prevent electrode degradation and to enhance adhesion of the substrate with the PDMS after exposure to air plasma. To improve separation efficiency, the FIDTs were arranged at a  $60^\circ$  angle relative to the centre line of  $200\mu\text{m}$  wide,  $24.6\mu\text{m}$  high straight microfluidic PDMS channel.

Polystyrene particles (Magsphere, Pasadena, CA, USA) homogeneously suspended in solution (water diluted with 0.2% of Polyethylene Glycol (PEG)), were continuously injected into the microfluidic chamber through a  $20\mu\text{m}$  wide perpendicular injection channel, by a syringe pump (KDS100, KD Scientific, Holliston, MA, USA). The electrical signal required to excite the SAWs was produced by an RF signal generator (Rohde & Schwarz HAMEG HM8134-3), amplified (Research (25A250A)) and applied to the opposing FIDTs. The experiments were conducted on the stage of a fluorescence microscope (Olympus BX43) with a light source (Olympus U-RFL-T) and imaged using a PixeLink (PL-B782U usb2) digital CCD colour camera.

### Numerical simulation

The forces acting on a particle suspended in an acoustic field can be obtained analytically from knowledge of the pressure field, provided the particle's size is much smaller than the acoustic wavelength.<sup>60, 61</sup> In this study, effects of standing surface acoustic waves (SSAW) on particles with sizes approaching half of the SAW wavelength are examined, for which a numerical

method is required. The key to the virtual membrane concept is the difference in the force fields experienced by particles with different dimensions with respect to the acoustic wavelength. In order to demonstrate the proposed concept, a simplified 2D COMSOL Multiphysics 5.0 model has been developed. Experimentally, a standing acoustic pressure field is generated by the use of a pair of opposing FIDTs. Whilst a full 3D model of this would be desirable, it is not practical due to enormous computational cost. The 2D model employed, however, is sufficient to clearly demonstrate the trends in the acoustic force field magnitude as the particle size approaches half an acoustic wavelength while minimizing computational load. The model consists of a fluid filled chamber, at each end of which the boundaries act as a radiating pressure source. These boundaries have a curved profile to mimic the production of a focused standing acoustic pressure field (Fig 2) imposed by the FIDTs. The acoustic wavelength used in the numerical simulations are equated to that of the experimentally applied SAW wavelength  $\lambda_{\text{SAW}}$ .

The presence of a particle in an acoustic field scatters and diffracts incident sound waves. To avoid multiple reflections of the scattered component, matched impedance boundary conditions were imposed on the upper and lower edges of the fluid volume, mimicking the continuous channel used experimentally. In order to simulate the acoustic energy loss due to SAW amplitude decay along the substrate/fluid interface, the model incorporates acoustic attenuation ( $\alpha_{\text{SAW}} = 1/(9.2 \times \lambda_{\text{SAW}})$  Nepers/m).<sup>62</sup> Having imposed the conditions required to generate a representative pressure field, the acoustic radiation force (ARF) exerted on a compressible particle is calculated<sup>59, 63</sup> using:

$$F_{\text{rad}} = \frac{1}{2} \rho_f \int_{s_0} \left[ \langle v_1^2 \rangle - \frac{1}{\rho_f^2 c_f^2} \langle p_1^2 \rangle \right] n dS - \rho_f \int_{s_0} \langle (n \cdot v_1) v_1 \rangle dS \quad (1)$$

here  $\rho_f$  and  $C_f$  represent the density and sound speed of the fluid with values of  $1000\text{ kg/m}^3$  and  $1490\text{ m/s}$ , respectively, for water. The parameters  $\langle p_1^2 \rangle$  and  $\langle v_1^2 \rangle$  are the mean square fluctuation of the pressure and velocity respectively. The values for polystyrene fluorescent particles include density ( $\rho_p$ ) of  $1050\text{ kg/m}^3$  and speed of sound ( $C_p$ ) of  $2350\text{ m/s}$ . In line with previous studies, for the purpose of modelling the acoustic forces the fluid is assumed to be inviscid. The radiation forces calculated, as obtained from the numerical model in COMSOL, have been benchmarked against cases studied by Dual et al.<sup>63</sup> The spatial variation in the forces (x and y components) are found by moving the particles to various locations, this is done along defined lines of interest over a distance of  $\lambda_{\text{SAW}}$  with a step size of  $\lambda_{\text{SAW}}/9$ . Particles in a standing wave field that are denser and stiffer than the surrounding medium will migrate to the pressure nodes; forces are therefore examined along the line (AB) in Fig. 3a that cuts through the nodes and antinodes of the standing wave. Furthermore, for a standing wave with lateral intensity variation, small particles can be expected to migrate towards pressure nodes, but also towards lateral location along which there is maximum pressure fluctuation,<sup>37</sup> which occurs here at the centre of our focussed field. To explore how this behaviour varies with particle size, the second line of

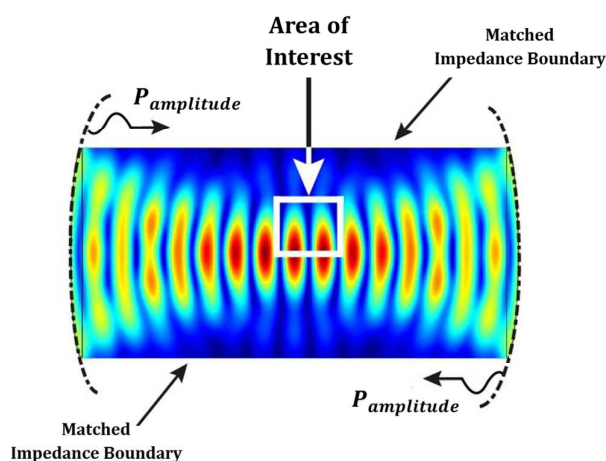


Fig. 2: FEA model of the system illustrating the 2<sup>nd</sup> order time averaged absolute pressure distribution as well as the applied boundary conditions. Area of interest depicts the region where the lateral forces are evaluated.

interest is defined as being along the length of the central pressure node (Line CD in Fig 3a).

## Results and discussions

### Numerical results

Particles are brought towards the edge of acoustic field by the fluid flow. With an initial random distribution across the width of the channel, they can encounter any part of the standing wave from node to antinode; as such the forces have been calculated along line AB (Fig 3a) which stretches from one antinode to the next.

The forces are derived from Eq. 1 and are the integral of forces on the surface of the particles shown in Fig. 3 (b) and (c). The results are shown in Fig 3 (d) and (e) for the forces in the x (along AB) and y (along CD) directions respectively. Fig 3d demonstrate that the forces in the x-direction act to move the particles towards the pressure node regardless of particle size (over the range examined), though the magnitude of these forces does vary. The force components in the y direction (perpendicular to the nodes), as shown in Fig 3e for particles located along AB; however, show a variation in both magnitude and sign. For the case of the smaller 2  $\mu\text{m}$  particle, the force fluctuates in sign along AB, becoming negative (directed into the sound field) as the particle approaches the nodal position. As such smaller particles are pushed laterally towards the node, a location at which they are then drawn into the acoustic field. This is in agreement with analytical expressions and experimental data for particles substantially smaller than the wavelength<sup>36</sup>. However, the force acting on the 10 and 5  $\mu\text{m}$  particles ( $\lambda_{\text{SAW}} = 20 \mu\text{m}$ ) is positive along the whole length of AB, and as such acts to prevent the particles from entering the sound field.

The force field is further examined by considering the forces along line CD in the y-direction (in the x-direction they are as close to zero as allowed numerically). As shown in Fig 3f, the smaller particles are drawn to the location  $y = 0$  along the nodal line, again in line with expectations<sup>36</sup>. However, a positive (repulsive) force, is shown to be present along the length of line CD for larger particles, preventing them from travelling along the node.

The simulations show that the sound field will repulse particles whose dimensions approach the half wavelength of the acoustic field, and can thus counteract flow induced fluid drag. To define what is meant by a "larger" particle, Fig 3g shows the value of  $F_y$  at a single location along CD for varying particle diameters (scaled based on each of the three wavelengths used). The data for each wavelength doesn't collapse onto a single line due to wavelength dependent differences in the degree of lateral focussing in the sound field. For each of the wavelengths at low particle sizes the force is negative, i.e. the particle is drawn into the field, whilst for larger particle sizes this becomes positive indicating rejection from the field. The cross over in the sign of the force occurs over the range of  $D(\lambda_{\text{SAW}}/2)^{-1}$  between 0.22 and 0.27, for the two dimensional particles modelled. Above these values, the forces rise rapidly with particle size. This indicates the possibility of sorting when

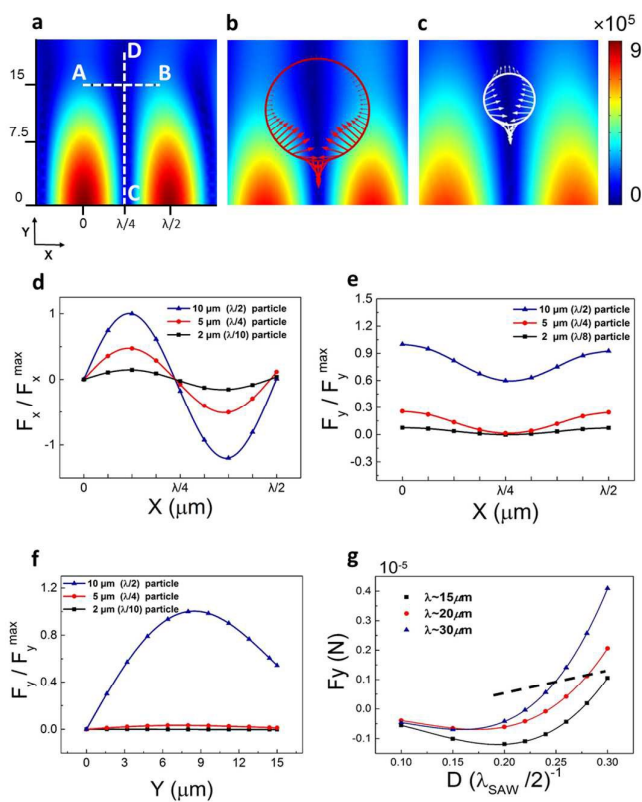


Fig. 3: (a) FEA model of the 2<sup>nd</sup> order time averaged absolute pressure distribution ( $\lambda_{\text{SAW}} = 20 \mu\text{m}$ ) with no particle present.  $\lambda$  here represent  $\lambda_{\text{SAW}}$ . The dashed black line (AB) (from  $x = 0$  to  $x = \lambda/2$  at  $y = 15 \mu\text{m}$ ) represents the path across which the spatial forces acting on particles have been assessed. (b) Spatial force field with a (b) 10 and (c) 5  $\mu\text{m}$  particle. The resultant forces, once integrated over the surface area are shown in (d) x component of the lateral force, normalized by the maximum  $F_x$  along the dashed line (AB) shown in part a. (e) y component of the lateral force, normalized by the maximum  $F_y$  along the dashed line (AB). (f) y component of the lateral force, normalized by the maximum  $F_y$  along the pressure minima line (CD). The y component (g) of the acoustic force acting on a particle at a single location along CD, shows a transition between negative (acceptance into the sound field) and positive (rejection from the sound field) forces at approximately  $D(\lambda/2)^{-1} = 0.3$ . The repulsive force rises rapidly with increasing particle diameter, as does a fluid flow induced drag that is of a similar magnitude to the acoustic forces – here notionally shown as the dotted line at a strength equal to that of a 8  $\mu\text{m}$  particle and proportional to radius. Smaller particles are drag dominated and larger ones are acoustic force dominated, giving rise to the possibility of filtering.

combined with fluid flow induced drag, when the strength of the acoustic field and flow field is such that the acoustic force of similar or greater magnitude to that induced by fluid drag. We have considered this scenario in Fig 3g, in which the dotted line represents the notional drag force, the amplitude of which is selected to cross the line (for  $\lambda_{\text{SAW}} = 20 \mu\text{m}$ ) at the point corresponding to an example 8  $\mu\text{m}$  particle. The dotted line is constantly sloped as the drag force is proportional to particle diameter. Two outcomes are predicted by this scenario, the first is for particles larger than 8  $\mu\text{m}$  for which the acoustic repulsion force is larger than the drag force, so that the particles are prevented from traversing the acoustic field, the second is for particles smaller than 8  $\mu\text{m}$  for which the drag force is dominant

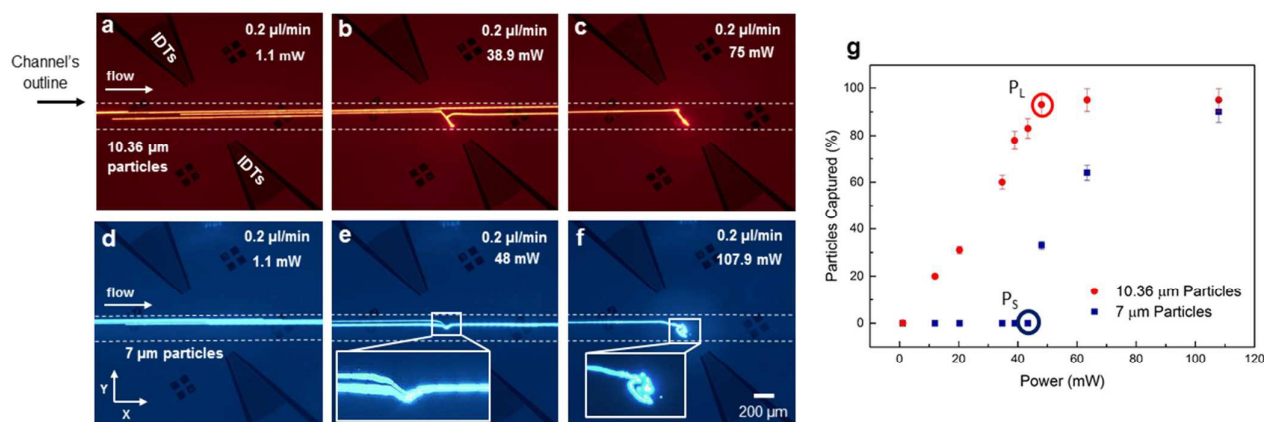


Fig.4. Experimental images of particle manipulation and sorting efficiency at different applied powers. These show optical fluorescent images of 10.36  $\mu\text{m}$  particles (a-c) where (a) particles are not affected by the field at 1.1 mW applied power, (b)  $78 \pm 3.9\%$  of particles at 38.9 mW applied power and (c)  $95 \pm 5\%$  of particles at 75 mW applied power (all with 0.2  $\mu\text{l}/\text{min}$  lateral flow rate) are trapped/filtered once they reach the field. Sorting behaviour of 7.0  $\mu\text{m}$  particles is shown in Fig (d-f) where these particles (d) continue in the direction of the flow at 1.1 mW applied power (e) are laterally displaced upon entering the field as they are affected by the acoustic force (f) are trapped at the start of the field as they are subjected to acoustic streaming and move along circular paths. (g) Capture efficiency as a function of power, with higher power resulting in greater capture efficiency; the cut-off power is where greatest number of larger particles are captured while smaller particles are able to pass through the field (circled).  $P_L$  and  $P_S$  represent powers at which  $95 \pm 5\%$  of large and  $5 \pm 5\%$  of smaller particles are captured respectively. These powers are utilized to obtain the results shown in Fig.5.

where these particles migrate to the local nodal locations by  $F_x$  and are dragged through the sound field along the nodal lines. It is this alignment of the smaller particles along the nodes as they pass through the field which is reminiscent of a series of filtering pores.

### Experimental results

Having established the underlying mechanism via numerical simulation, we now demonstrate selective trapping of particles experimentally. Fig 4 illustrates the difference in behaviour of 7  $\mu\text{m}$  and 10.36  $\mu\text{m}$  particles separately (blue and red, respectively), which enter (from the left) a sound field with a surface acoustic wavelength of 20  $\mu\text{m}$ . At very low powers (Fig 4a, d) neither particle size is affected by the sound field, instead the viscous drag forces ( $F_{drag} = 6\pi\mu rU$ ; where  $r$  is the particle radius,  $\mu$  the viscosity and  $U$  the relative velocity of the particle and fluid) imposed by the flowing fluid are dominant. However, when the applied acoustic force is sufficient to counter the fluid drag forces for the larger particles, it is observed that when they reach the standing acoustic pressure field, particles are trapped at its periphery, as predicted by the positive nature of  $F_y$  in Fig 3 e, f. In addition, influenced by the drag of the fluid and the fact that the sound field has been angled towards the flow field, they are collected at the lower (in the image plane) edge of the channel (Fig 4 b, c). In contrast, at low powers (Fig 4e) the smaller particles are able to be drawn into the force field, along the nodal lines – seen be a clear perturbation in the trajectory. Once at the nodes the fluid viscous drag force draws them through the field and along the channel. As the applied power is further increased the smaller particles can also be captured, this occurs due to a different mechanism than that used to capture the larger particles. For these smaller particles the trapping results in particle clusters which are in constant motion, which indicates that the particles are located in a vortex induced by acoustic streaming<sup>44, 64</sup> (Fig 4f). The effect of streaming wasn't included in the model as it would require a 3D model which is currently computationally prohibitive, instead this is

characterised experimentally. Fig 4g quantifies the role that the applied power plays in the capturing of each particle size. It can be seen that, at the higher applied power levels and concordant higher acoustic pressure amplitudes, the magnitude of lateral acoustic forces becomes more dominant compared to the drag force for the larger particles (10.36  $\mu\text{m}$ ), hence a larger proportion are captured; 75 mW is sufficient to trap  $95 \pm 5\%$  of the particles (where the uncertainty is one standard error). For low powers, the smaller particles (7  $\mu\text{m}$ ) aren't trapped in the force field, however, above a certain power level (50mW) their trajectories become increasingly dominated by fluid drag resulting from acoustic streaming. These data sets suggest that selective trapping can be achieved at powers between 43.4 mW (where  $83 \pm 4.15\%$  of 10  $\mu\text{m}$  particles are

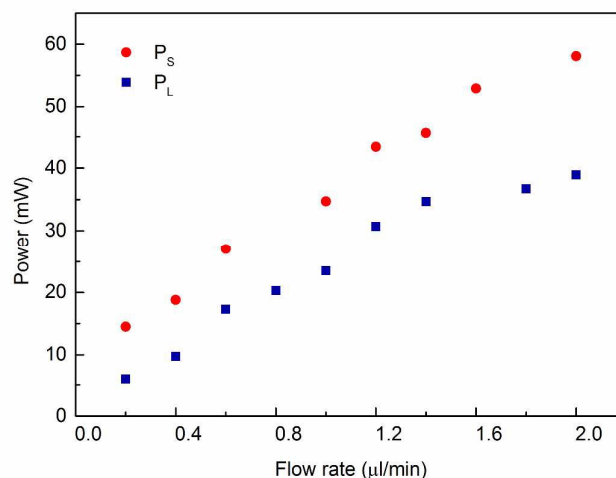


Fig.5. Applied power as a function of flow rate. As shown in Fig. 4,  $P_S$  indicates the power at which  $95 \pm 5\%$  of smaller particles (7 $\mu\text{m}$ ) are able to pass through the force field whilst  $85 \pm 5\%$  of the larger particles (10.36 $\mu\text{m}$ ) get trapped.  $P_L$ , on the other hand, is the power to capture the larger particles and allow  $75 \pm 5\%$  of particles of smaller diameter to be drawn into the force field without being interrupted by the streaming induced drag force.

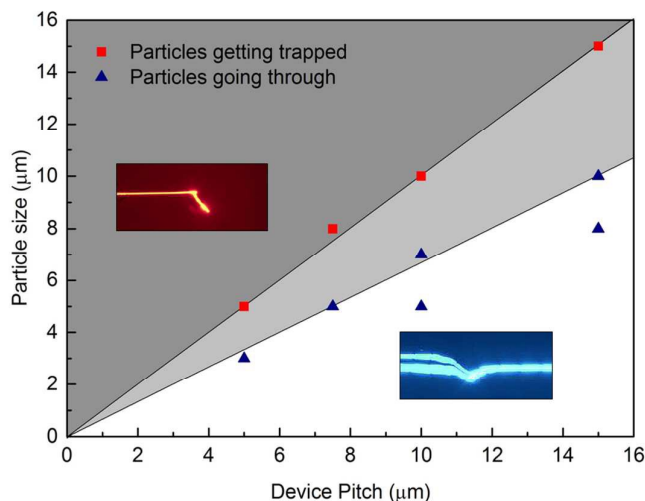


Fig. 6: The effective critical particle diameter is a function of the acoustic wavelength. The cut off in behaviour is examined here across multiple device pitches ( $\lambda_{\text{SAW}}/2$   $\mu\text{m}$ ). Particles within the dark grey area are trapped statically, with the red squares being the smallest particles to be captured. The slope of the line, separating the dark grey area was found to be very close to 1. Particles located in the light grey area show a mixture of behaviour. In the white section, particles are able to pass through the field at powers at which the larger particles are trapped.

captured whilst 100 % of smaller particles pass through the acoustic pores) and 49 mW (where  $95 \pm 5$  % of 10  $\mu\text{m}$  particles are captured, but only  $36 \pm 3.2$  % of smaller 7  $\mu\text{m}$  particles pass through).

Fig 5 further investigates the influence of power, as a function of flow rate, on desired capture and separation of particles. Two parameters have been defined;  $P_L$ , the lowest power at which all of the large particles are trapped, and  $P_S$  the highest power at which the small particles pass through the field. It can be seen that the difference in these values at 0.2  $\mu\text{l}/\text{min}$ , the flow rate used in Fig 4, remains the same up to in excess of 1.0  $\mu\text{l}/\text{min}$ .

Because the sorting efficiency is dependent on the similarity of  $P_S$  and  $P_L$ , it is beneficial for the transition from 0% to 100% capture of a given particle type to take place over a narrow power range; if the slope along which the red squares are located in Fig 4g were less steep,  $P_L$  would be larger and the sorting efficiency lower. Similarly, Fig 4 g demonstrates that the capture rate for increasing applied power is steeper for larger particles (acoustic radiation force trapped) than the smaller ones (acoustic streaming trapped); an increase of 50 mW in power is needed to increase the collection by streaming from 65% to 90%. In streaming fields, the movement of the particles leads to particle-particle and particle-wall interactions that can lead to particles being expelled out of the streaming vortex,<sup>64</sup> possibly responsible for the relatively inefficient collection for the streaming based mechanism relative to that induced by the acoustic force. Accordingly, acoustic radiation forces are the preferential particle capture mechanism. In Fig 6, four individual devices have been examined with pitches of 5  $\mu\text{m}$ , 7.5  $\mu\text{m}$ , 10  $\mu\text{m}$  and 15  $\mu\text{m}$  ( $\lambda_{\text{SAW}} = 10, 15, 20$  and 30  $\mu\text{m}$ ). In each device we varied the power whilst examining which particle sizes could be captured. This was possible for the larger particle sizes marked with red squares (located within the dark grey area), and not for those smaller particles shown with

blue triangles (located in the white area). Then a power was found at which the larger particles were captured for each experimental condition, whilst the smaller ones passed through the field – the two insets show this occurring. Interestingly it can be seen that for particles held statically, they must have a diameter which is greater than the pitch of the IDTs. Whilst the mechanism for this is not understood, the experimental characterisation gives rise to a simple design rule for these sorting devices and the mechanism can be considered to be tuneable based on IDT pitch.

The number of particles that can be successfully trapped, even for those larger than half the acoustic wavelength, is limited by volumetric constraints as the bolus of trapped particles extends across the channel width. Whilst the devices presented here have not been optimised for maximum particle capture, they can give an indication of the limitations involved. As small particles enter the channel at the edge of the channel, which can be arranged simply with a buffer flow, the trajectories can be seen in Fig 7 b; the small particles pass through the centre part of the channels, as with any membrane when the larger particle obstructs the pathway of the smaller particles, filtration performance is hindered. As such, the bolus must be limited in size such that it doesn't hinder this trajectory, the number of 10  $\mu\text{m}$  particles (the largest used in these experiments) trapped is plotted against the height of the bolus in Fig 7 a, the volume of these trapped particles represents almost perfect packing. Clearly, additional trapping capacity would be expected with

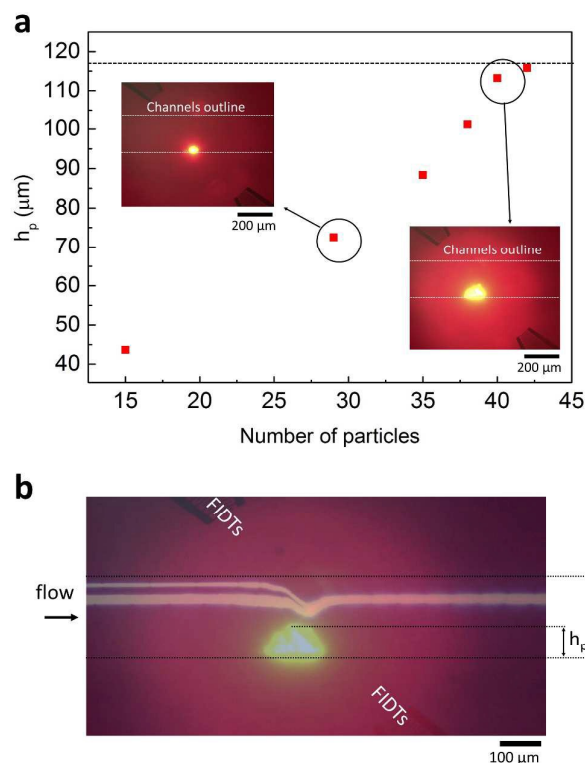


Fig. 7: (a) As time progresses the size of the bolus of 10.36  $\mu\text{m}$  particles grows, the width across the channel is plotted against the number of particles captured (each data point is equally spaced temporally). (b) A composite image of the trajectories of small particles (7  $\mu\text{m}$ ) entering along the edge of the channel, and the growing bolus of large particles, once the tip of the bolus impedes this trajectory, the filter will cease to perform efficiently, the height at which that occurs is marked as a dotted line in (a).

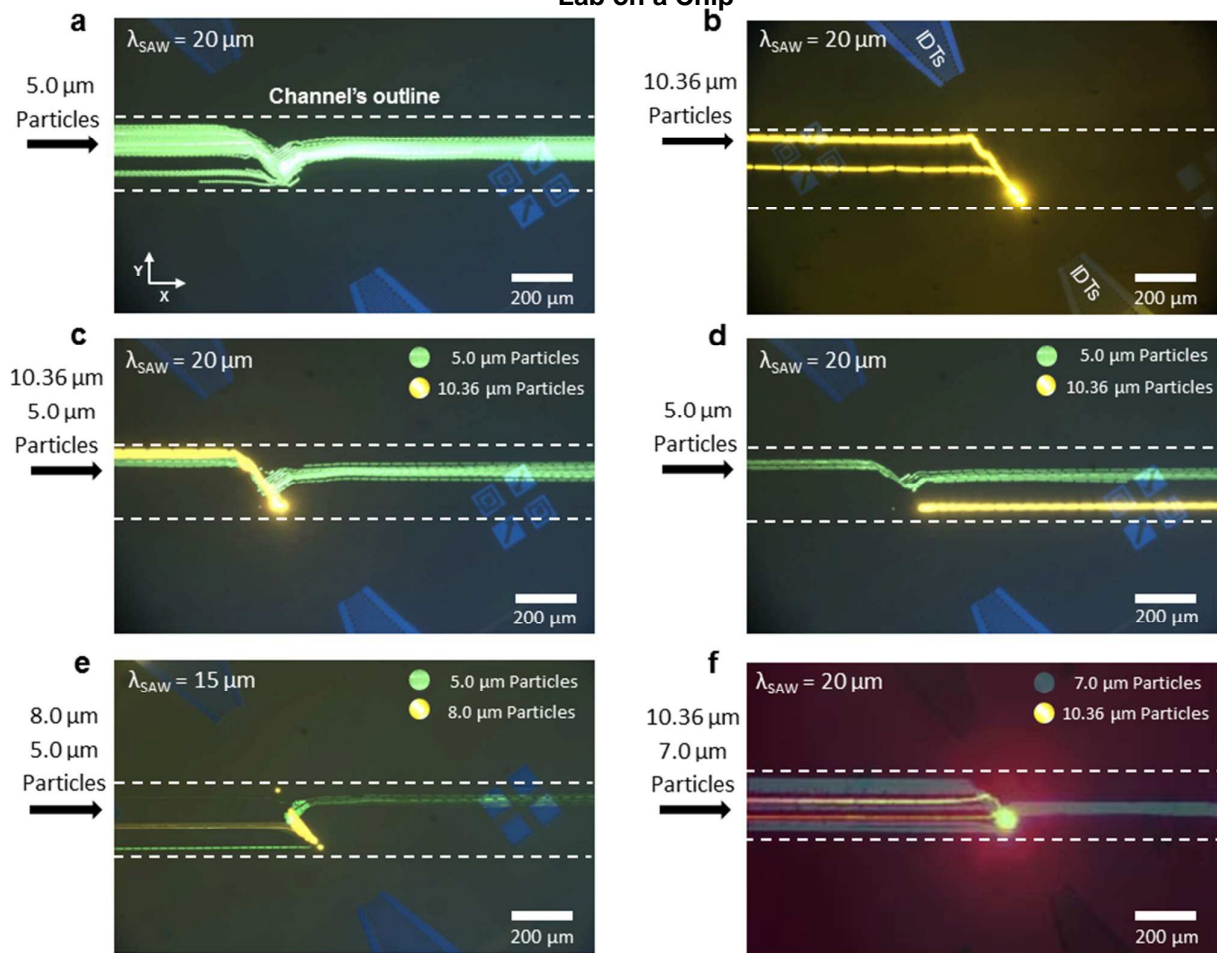


Fig 8. Particle sorting using an acoustic filter. Trajectories of fluorescent polystyrene particles of 5  $\mu\text{m}$  (green) and 10.36  $\mu\text{m}$  (yellow) diameter entering the microfluidic chamber at the flow rate of 2  $\mu\text{l}/\text{min}$  through the left side entrance. Here, the focused IDTs, composed of  $\lambda_{\text{SAW}}=20 \mu\text{m}$  finger-pairs operating at 194MHz, are acting at a 45° angle relative to the microfluidic channel. Once particles reach the standing acoustic pressure field (in the middle of the chamber), established by a pair of counter propagating SAW devices (a) particles of diameter  $D_p < D_{\text{critical}}$  are laterally displaced and pass through the potential force minima lines towards the upper edge of the chamber, then to the exit, (b) particles of  $D_p \geq D_{\text{critical}}$  are trapped at the last possible pressure nodes and are directed towards the lower edge of the chamber due to fluid drag. (c) The combination of these two sorting behaviours is illustrated where simultaneous separation of particles occurs. (d) Release of 10.36  $\mu\text{m}$  particles once the application of SAW is stopped, (e) separation of 8  $\mu\text{m}$  (yellow) and 5  $\mu\text{m}$  (green) particles with  $\lambda_{\text{SAW}}=15 \mu\text{m}$ . (f) Separation of 7  $\mu\text{m}$  (blue) and 10.36  $\mu\text{m}$  (red) particles using a  $\lambda_{\text{SAW}}=20 \mu\text{m}$  device in a composite picture of videos taken from the same device under identical experimental conditions.

wider channels, or potentially by offsetting the focal region of the acoustic field away from the centre of the channel to divert the trajectory of the small particles.

Particle sorting of mixed particle inputs is demonstrated Fig 8, including 10.36  $\mu\text{m}$  and 5.0  $\mu\text{m}$  particles (yellow and green), using a  $\lambda_{\text{SAW}}=20 \mu\text{m}$  wavelength device operating at 194. In Fig 8 (a) to (c) the applied power and flow rate have been specifically adjusted to capture the greatest number of larger particles ( $95 \pm 5\%$ ), whilst all the smaller particles pass through the field. As seen in Fig 8 (c), once the mixture consisting of 10.36  $\mu\text{m}$  and 5.0  $\mu\text{m}$  particles (flowing from left to right) arrive to the established standing pressure field, the larger particles are selectively retained. As discussed previously and as indicated in the numerical model, the larger 10.36  $\mu\text{m}$  particles are captured and follow the outer edge of the sound field (inclined to the flow field) to the lower edge of the chamber, while the smaller 5.0  $\mu\text{m}$  particles pass through the sound field along the pressure nodes. Once the sound field is turned off, the trapped particles are released (Fig 8 d). The released larger particles will follow a path adjacent to the lower side of the chamber; as such they could be collected from

multiple outlets downstream. However, we envisage that the primary use of this function is the dispensing of the smaller particles from an open ended channel, followed by release and dispensing of the larger particles.

To emphasise the scalability of the system, in Fig 8 (e and f), different populations of mixed particle sizes are sorted: firstly 8  $\mu\text{m}$  particles are sorted from 5  $\mu\text{m}$  using a 15  $\mu\text{m}$  wavelength device, corresponding to a 7.5  $\mu\text{m}$  device pitch. Similarly, 10.36  $\mu\text{m}$  particles are sorted from 7  $\mu\text{m}$  ones using a device pitch of 10  $\mu\text{m}$  (in this case, a composite image consisting of two images is shown due to the need to switch optical filters).

## Conclusions

A deterministic SAW-based sorting and filtration mechanism has been demonstrated. It utilises high frequency standing acoustic pressure fields, established by the generation of counter propagating focussed surface acoustic waves. In the regime where the surface acoustic wavelength approaches that of the

particle diameter a novel behaviour has been identified and utilized for selective particle filtration. Particles smaller than a critical diameter, dictated by a balance between acoustic power and flow rate, are permitted to pass through the virtual pores formed at acoustic nodal locations translate through the field. Larger particles, however, are retained at the leading edge of the sound field by acoustic radiation forces.

## Acknowledgements

The authors would like to thank the Australian Research Council (No. DP160101263) for their kind support of this research. All devices used in this work were fabricated at the Melbourne Centre for Nanofabrication (MCN).

## References

1. B. Landenberger, H. Hofemann, S. Wadle and A. Rohrbach, *Lab on a chip*, 2012, 12, 3177-3183.
2. M. P. MacDonald, G. C. Spalding and K. Dholakia, *Nature*, 2003, 426, 421-424.
3. P. R. C. Gascoyne and J. Vykoukal, *Electrophoresis*, 2002, 23, 1973-1983.
4. S. Park, Y. Zhang, T. H. Wang and S. Yang, *Lab on a chip*, 2011, 11, 2893-2900.
5. H. Shafiee, M. B. Sano, E. A. Henslee, J. L. Caldwell and R. V. Davalos, *Lab on a chip*, 2010, 10, 438-445.
6. D. J. Collins, T. Alan and A. Neild, *Lab on a Chip*, 2014, 14, 1595-1603.
7. J. Nam, Y. Lee and S. Shin, *Microfluidics and Nanofluidics*, 2011, 11, 317-326.
8. J. Nam, H. Lim, D. Kim and S. Shin, *Lab on a chip*, 2011, 11, 3361-3364.
9. P. Li, Z. Mao, Z. Peng, L. Zhou, Y. Chen, P.-H. Huang, C. I. Truica, J. J. Drabick, W. S. El-Deiry and M. Dao, *Proceedings of the National Academy of Sciences*, 2015, 112, 4970-4975.
10. M. Hejazian, W. Li and N.-T. Nguyen, *Lab on a Chip*, 2015, 15, 959-970.
11. C. W. Shields IV, C. D. Reyes and G. P. López, *Lab on a Chip*, 2015, 15, 1230-1249.
12. J. Nam, H. Lim, C. Kim, J. Y. Kang and S. Shin, *Biomicrofluidics*, 2012, 6, 024120.
13. J. Shi, H. Huang, Z. Stratton, Y. Huang and T. J. Huang, *Lab on a chip*, 2009, 9, 3354-3359.
14. F. Petersson, A. Nilsson, C. Holm, H. Jonsson and T. Laurell, *Lab on a chip*, 2005, 5, 20-22.
15. X. Ding, Z. Peng, S. C. Lin, M. Geri, S. Li, P. Li, Y. Chen, M. Dao, S. Suresh and T. J. Huang, *Proceedings of the National Academy of Sciences* 2014, 111.
16. J. Behrens, S. Langelier, A. R. Rezk, G. Lindner, L. Y. Yeo and J. R. Friend, *Lab on a chip*, 2015, 15, 43-46.
17. F. Beyeler, A. Neild, S. Oberti, D. J. Bell, Y. Sun, J. Dual and B. J. Nelson, *Journal of Microelectromechanical systems* 2007, 12.
18. A. Neild, S. Oberti, F. Beyeler, J. Dual and B. J. Nelson, *Journal of Micromechanics and Microengineering*, 2006, 16, 1562-1570.
19. P. J. Lee, P. J. Hung, R. Shaw, L. Jan and L. P. Lee, *Applied Physics Letters*, 2005, 86, 223902.
20. D. J. Grier, *Nature*, 2003, 424.
21. A. H. Yang, S. D. Moore, B. S. Schmidt, M. Klug, M. Lipson and D. Erickson, *Nature*, 2009, 457, 71-75.
22. E. Mirowski, J. Moreland, S. Russek, M. Donahue and K. Hsieh, *Journal of Magnetism and Magnetic Materials*, 2007, 311, 401-404.
23. E. Mirowski, J. Moreland, A. Zhang, S. E. Russek and M. J. Donahue, *Applied Physics Letters*, 2005, 86, 243901.
24. D. J. Collins, T. Alan and A. Neild, *Applied Physics Letters*, 2014, 105, 033509.
25. S. Oberti, D. Moller, A. Neild, J. Dual, F. Beyeler, B. J. Nelson and S. Gutmann, *Ultrasonics*, 2010, 50, 247-257.
26. P. Rogers and A. Neild, *Lab on a chip*, 2011, 11, 3710-3715.
27. D. J. Collins, B. Morahan, J. Garcia-Bustos, C. Doerig, M. Plebanski and A. Neild, *Nature Communications*, 2015, 6.
28. M. Wiklund, *Lab on a chip*, 2012, 12, 2018-2028.
29. D. Bazou, R. Kearney, F. Mansergh, C. Bourdon, J. Farrar and M. Wride, *Ultrasound in medicine & biology*, 2011, 37, 321-330.
30. J. Hultstrom, O. Manneberg, K. Dopf, H. M. Hertz, H. Brismar and M. Wiklund, *Ultrasound in medicine & biology*, 2007, 33, 145-151.
31. B. T. Chu and R. E. Apfel, *The Journal of the Acoustical Society of America*, 1982, 72, 1673-1687.
32. D. J. Collins, T. Alan, K. Helmerson and A. Neild, *Lab on a Chip*, 2013, 13, 3225-3231.
33. I. Leibacher, P. Reichert and J. Dual, *Lab on a Chip*, 2015, 15, 2896-2905.
34. I. Leibacher, S. Schatzer and J. Dual, *Lab on a Chip*, 2014, 14, 463-470.
35. P. Hahn, I. Leibacher, T. Baasch and J. Dual, *Lab on a Chip*, 2015, 15, 4302-4313.
36. M. Antfolk, P. B. Muller, P. Augustsson, H. Bruus and T. Laurell, *Lab on a Chip*, 2014, 14, 2791-2799.
37. A. Neild, S. Oberti and J. Dual, *Sensors and Actuators B: Chemical*, 2007, 121, 452-461.
38. A. Neild, S. Oberti, A. Haake and J. Dual, *Ultrasonics*, 2006, 44 Suppl 1, e455-460.
39. P. Glynn-Jones, C. E. Demore, C. Ye, Y. Qiu, S. Cochran and M. Hill, *IEEE transactions on ultrasonics, ferroelectrics, and frequency control*, 2012, 59, 1258-1266.
40. M. Antfolk, C. Magnusson, P. Augustsson, H. Lilja and T. Laurell, *Analytical chemistry*, 2015.
41. P. Augustsson, C. Magnusson, M. Nordin, H. Lilja and T. Laurell, *Analytical chemistry*, 2012, 84, 7954-7962.
42. F. Petersson, L. Åberg, A.-M. Swärd-Nilsson and T. Laurell, *Analytical chemistry*, 2007, 79, 5117-5123.
43. D. J. Collins, A. Neild and Y. Ai, *Lab on a chip*, 2016, 16, 471-479.
44. D. J. Collins, Z. Ma and Y. Ai, *Anal Chem*, 2016, 88, 5513-5522.
45. M. Sesen, T. Alan and A. Neild, *Lab Chip*, 2014.
46. L. Schmid and T. Franke, *Applied Physics Letters*, 2014, 104, 133501.
47. M. Sesen, T. Alan and A. Neild, *Lab on a chip*, 2015, 15, 3030-3038.
48. C. Cortez-Jugo, A. Qi, A. Rajapaksa, J. R. Friend and L. Y. Yeo, *Biomicrofluidics*, 2015, 9, 052603.
49. K. Tveen-Jensen, F. Gesellchen, R. Wilson, C. M. Spickett, J. M. Cooper and A. R. Pitt, *Scientific reports*, 2015, 5.
50. D. J. Collins, O. Manor, A. Winkler, H. Schmidt, J. R. Friend and L. Y. Yeo, *Physical Review E*, 2012, 86, 056312.

51. L. Ren, Y. Chen, P. Li, Z. Mao, P.-H. Huang, J. Rufo, F. Guo, L. Wang, J. P. McCoy and S. J. Levine, *Lab on a Chip*, 2015, 15, 3870-3879.
52. A. A. Nawaz, Y. Chen, N. Nama, R. H. Nissly, L. Ren, A. Ozcelik, L. Wang, J. P. McCoy, S. J. Levine and T. J. Huang, *Analytical chemistry*, 2015.
53. R. Shilton, M. K. Tan, L. Y. Yeo and J. R. Friend, *Journal of Applied Physics*, 2008, 104, 014910.
54. A. R. Rezk, A. Qi, J. R. Friend, W. H. Li and L. Y. Yeo, *Lab on a Chip*, 2012, 12, 773-779.
55. L. Schmid, D. A. Weitz and T. Franke, *Lab on a Chip*, 2014, 14, 3710-3718.
56. V. Skowronek, R. W. Rambach, L. Schmid, K. Haase and T. Franke, *Analytical chemistry*, 2013, 85, 9955-9959.
57. J. Shi, X. Mao, D. Ahmed, A. Colletti and T. J. Huang, *Lab on a chip*, 2008, 8, 221-223.
58. G. Destgeer, B. H. Ha, J. H. Jung and H. J. Sung, *Lab on a Chip*, 2014, 14, 4665-4672.
59. C. Devendran, N. R. Gunasekara, D. J. Collins and A. Neild, *RSC Advances*, 2016, 6, 5856-5864.
60. L. P. Gor'kov, *Soviet physics Doklady*, 1962, 6, 773.
61. M. Settnes and H. Bruus, *Physical Review E*, 2012, 85, 016327.
62. S. Shiokawa, Y. Matsui and T. Ueda, *Ultrasonic Symposium* 1989.
63. J. Dual, P. Hahn, I. Leibacher, D. Moller, T. Schwarz and J. Wang, *Lab on a chip*, 2012, 12, 4010-4021.
64. H. V. Phan, M. Şeşen, T. Alan and A. Neild, *Applied Physics Letters*, 2014, 105, 193507.